PROCESS-STRUCTURE-PROPERTY RELATIONSHIP OF MICRO-CHANNEL TUBE FOR CO_2 CLIMATE CONTROL SYSTEMS

A thesis presented to the faculty of the

Fritz J. And Dolores H. Russ College of Engineering and Technology of

Ohio University

In partial fulfillment

of the requirements for the degree

Master of Science

Gowreesan Vamadevan

November 2004

This thesis entitled

PROCESS-STRUCTURE-PROPERTY RELATIONSHIP OF MICRO-CHANNEL TUBE FOR CO_2 CLIMATE CONTROL SYSTEMS

by

GOWREESAN VAMADEVAN

has been approved for
the Department of Mechanical Engineering
and the Russ College of Engineering and Technology by

Frank Kraft

Assistant Professor of Mechanical Engineering

Dennis Irwin

Dean, Russ College of Engineering and Technology

VAMADEVAN, GOWREESAN. M.S. November 2004 Mechanical Engineering

Process-Structure-Property Relationship of Micro-channel tube for CO_2 Climate Control Systems (71pp.)

Director of Thesis: Frank Kraft

As the operating conditions of climate control systems become strenuous due to the switching to the CO_2 refrigerant, the mechanical properties of micro channel tubing used for heat transfer become crucial. Because of the processes involved in the manufacturing and assembling of the heat exchangers, the microstructure of the tube changes. Hence the mechanical properties of the tubing are different from that of raw materials. An apparatus to measure mechanical properties of the tubing under simulated working conditions was designed and fabricated. Using the apparatus, the responses of the tubing under static and cyclic loading conditions are analyzed at different temperatures. In addition, the response due to cyclic loading with hold times at maximum and minimum pressures are analyzed. The data are to be used for the designing of micro channel tubing for heat exchangers for climate control systems with CO_2 refrigerant.

Approved:

Frank Kraft

Assistant Professor of Mechanical Engineering

ACKNOWLEDGMENTS

I would like to express my sincere gratitude and appreciation to my adviser Dr. Frank Kraft for his continuous guidance and encouragement in gearing me with this work. I am thankful for Dr.Hajrudin Pasic and Dr.Daniel Gulino for their guidance and for being the members of my thesis committee. Work of Mr. Leonard Huffman, laboratory coordinator, is also appreciated.

Industrial sponsors of this work were Brazeway, Inc. of Adrian, Michigan and Erbsloeh Aluminium GmbH of Velbert, Germany. The author is thankful to these companies for their financial support and for providing the test samples and conducting chemical analyses. This work was also partially funded by the Ohio University Office of Research and Sponsored Programs through an OURC (Ohio University Research Committee) grant, and the Russ College of Engineering and Technology

TABLE OF CONTENTS

LIST OF FIGURES

LIST OF TABLES

CHAPTER 1

INTRODUCTION

The replacement of conventional refrigerants with CO_2 (R744) demands more mechanical performance from the components of the climate control system specifically operating pressure and temperatures are significantly greater than that of systems with conventional refrigerants. Hence the mechanical design and testing of the components of the climate control system become important. In this work, an apparatus was designed and built to measure the mechanical properties of aluminum alloy micro channel tubes used in climate control systems with CO_2 refrigerant. Based on the results from the testing with this apparatus, the process-structure-property relationship of micro channel tube for climate control systems with CO_2 refrigerant was analyzed.

This first chapter presents background information about the work, the objectives of the work and the outline of the thesis report.

1.1 Background

Having realized that the R12 (Dichlorodifluoromethane) and other chlorofluorocarbons (CFC) used as refrigerants cause depletion in the ozone layer, more than 150 countries signed the Montreal protocol, a treaty to protect earth's ozone layer. The United States implemented this by the Clean Air Act, thus ending the production of CFC-12 for refrigeration and air conditioning [1]. The phase-out of R12 prompted the research to find environment-friendly refrigerants and more efficient climate control systems. Currently R134a is being widely used as a refrigerant in residential, commercial and vehicle air-conditioning systems. R134a is a fluorinated hydro fluorocarbon.

However research is being done with natural and non-flammable CO_2 (R744) designated as an alternate refrigerant due to several reasons.

1.2 Advantages of R744 as refrigerant

CO_2 as refrigerant is believed to have significantly less impact on the environment compared to R 134a. Quantitatively stated, the greenhouse potential of CO_2 is 1300 times lower than that of R134a [2]. Hence CO_2 systems simplify the serviceability for the dealers and automobile manufacturers [3].

In addition, the systems with CO_2 refrigerant perform better than systems with R134a as heat pumps. This is very important for hybrid or high efficiency vehicles where the heat output by the engine is very low. Researchers have shown that a CO_2 model could match conventional car air conditioning systems in addition to providing the highest heating capacity during coldest conditions. This property makes the system with R744 as the refrigerant, to be switched between heating mode and cooling mode.

Also researchers have shown that the heating capacity of systems with R744 as the working fluid is higher than that of residential systems using R410A as the working fluid at lower outdoor temperatures [4]. There is also some operational flexibility associated with climate control systems using R744 refrigerant. The first advantage is that the blower power can be reduced, as it is possible to have higher air exit temperature. The second advantage is that the set points can be reached quickly when experiencing air temperature drifts, by increasing the capacity while sacrificing efficiency. Emissions of CO_2 by using a climate control system operating with R134a refrigerant is 30% less than that of a system with R744 as refrigerant [5]. Emissions due to both increased fuel consumption and leaks in the systems are included in this evaluation. Also CO_2 is non-flammable and fire suppressant. It is classified as non-toxic and it is widely available [6].

Toyota has started Shecco™ (Sustainable Heating and Cooling with Natural CO_2) Technology for automobile climate control systems [7]. This technology was commercialized in hot water units in 2001. This was in the form of a hot water supply unit with a heat pump with CO_2 refrigerant.

1.3 A climate control system

A schematic diagram of a climate control system is shown in Figure 1.1.

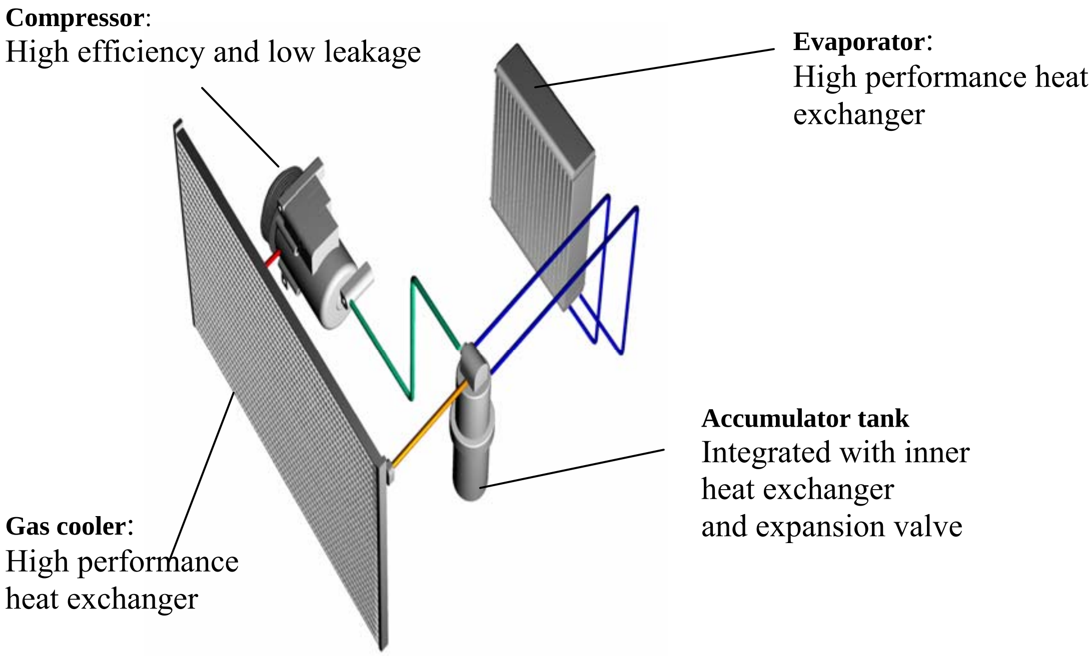

Figure 1.1: schematic diagram of a climate control system [8].

Both the evaporator and the gas cooler are heat exchangers in the system.

1.3.1 Evaporator

The purpose of the evaporator is to vaporize the refrigerant to remove the heat from the place or object to be cooled. The evaporator in a passenger compartment switches functions with the gas cooler when used as a heat pump.

1.3.2 Gas cooler

While the hot refrigerant vapor is pressurized and passed through the gas cooler, the heat from the refrigerant is transferred to the airflow due to fan or automobile motion. When used as a heat pump, this heat is used as required to heat the passenger compartment.

1.3.3 Micro channel tube

Micromultiport (MMP) tubing (also known as micro channel tube) is a flat body with a row of side-by-side channels separated by upright webs. Both automotive condensers and gas coolers are made from several micro channel unit slabs. Parallel tubes are connected to headers at both ends as shown in Figure 1.2(a). While the refrigerant passes through these tubes, heat transfer occurs. Fins are attached to the tubes to increase the heat transfer. The higher heat transfer performance is the main advantage of parallel flow micro channel heat exchangers.

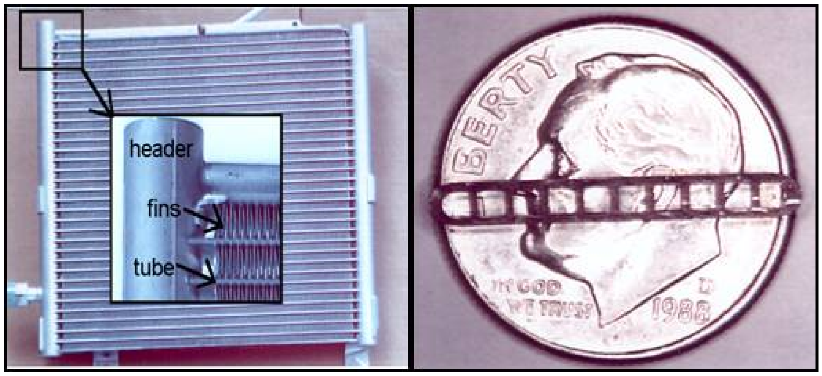

(a) **(b)**

Figure 1.2: The condenser into which MMP tubing is brazed and cross section of a generic MMP tubing in relation to a United States dime.

To demonstrate the size of MMP tube, a cross section of a generic 134a MMP design is shown with a United States dime in the Figure 1.2(b).

1.4 Proposed design criteria

Several prototypes of climate control systems (with extruded aluminum micro channel heat exchangers) with R744 as the refrigerant have been constructed by various institutions for research work (i.e, University of Illinois, SINTEF Energy Research Refrigeration and Air Conditioning- Trondheim, Norway, etc.). These researchers also produced data to propose material related design criteria and test methods for components of climate control systems driven with R744 as the refrigerant [2]. The table below gives the design conditions used for climate control systems using R134a and R744 as refrigerants [9, 10].

Table 1.1: Maximum operating conditions

	Systems driven by R134a	Systems driven by R744
Operating pressure (MPa) (maximum)	3	16
Operating temperature (C) (maximum)	125	180

As the service pressure and temperature are greater than that of previous refrigerants, the mechanical behavior and failure of the components of the unit becomes very important.

1.5 Manufacturing and assembling processes

The material undergoes several mechanical and thermal processes before being put into operation and as a result of these processes, the mechanical properties of the material change.

1.5.1 Extrusion of micro channel tubing

First a high quality homogenized billet of specified alloy is hot extruded. AA 1000 and AA 3000 series alloys are widely used. AA 1000 series alloys have aluminum contents of 99% or higher. Iron and silicon are the major impurities. AA 3000 series alloys have manganese as the major alloying element. These series are used for micro channel due to their high thermal conductivity, corrosion resistance and excellent workability [11].

Extrusion is the process of producing long straight parts of uniform cross section. This is done by placing a heated metal billet inside a container and forcing the billet through a die. This process can produce parts with solid and hollow sections. For mass production of aluminum micro channel tubing, this process offers tooling economy and energy savings.

As the webs of the tubing are very small, any voids or inclusions might reduce the strength of the tubing significantly. Therefore it is important to start with a high quality homogenized billet. Tight quality control is exercised on extruded tubing. Vision inspection of dimensions, burst pressure testing, laser measurements and on-line inspection are some of the methods applied for quality control.

Since extrusion is a continuous process, the tubing is wound onto coils as they are extruded. Then they are straightened, roll-sized and cut into required lengths. It is at this point when precise required external dimensions are achieved. The material handling process and roll sizing process introduce a small amount of cold-work in the tubing.

1.5.2 Nocolok® Brazing

This is the process of joining the tubing with two headers at both ends of the equal length tubing and fins to the tubes. A number of these pieces are assembled into condenser cores with fin stock and headers cladded with a brazing alloy. The assembly is then placed inside a furnace in a nitrogen environment. The brazing alloy has a melting point considerably lower than that of the material of the tubing. Brazing is done between 600-605C (approximately 94% of melting point of the alloy). At this temperature range, the brazing material melts but the micro channel tube does not. As a result of this process, the brazing material forms a metallurgical bond joining the surfaces of the component of the heat exchanger. This is done in an inert gas nitrogen environment to prevent oxidization and allow brazing to take place. The process, which is conducted in a controlled atmosphere, and uses a non-corrosive flux is known in the industry as Controlled Atmospheric Brazing (CAB) or NOCOLOK® brazing [12]. In this research work, the thermal brazing cycle was simulated in a laboratory furnace to obtain the same microstructure to study the effect of brazing.

1.5.3 Change in properties

As a result of these processes, the metallurgical structure such as grain size changes, resulting in a change in mechanical properties. Since grain size has a profound effect on mechanical properties, this results in a change in material properties. It has been shown that the small amount of cold work due to material handling and roll sizing affects the recrystalization and grain growth during brazing [13].

Figure 1.3 shows the change in grain structure due to simulated thermal brazing cycle. Figure 1.3 (a) shows the grain structure of the external and internal walls (webs) of a micro channel tube before simulated thermal brazing cycle. Figure 1.3 (b) shows grain structure after the simulated thermal brazing cycle.

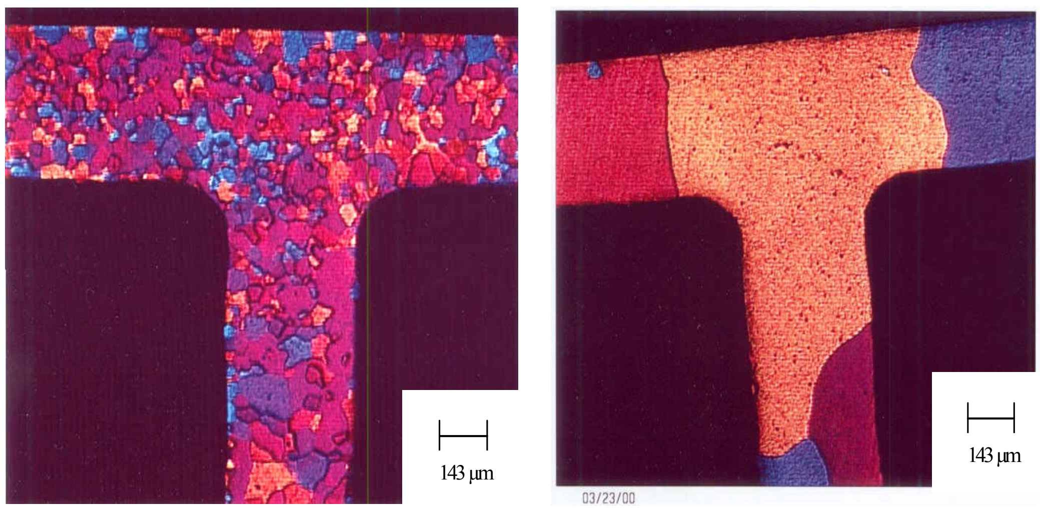

(a) **(b)**

Figure 1.3: Grain structure of MMP tubing before (a) and after (b) simulated thermal brazing cycle [13].

A change from the current R134a refrigerant to R744 results in operating conditions that will place the micro channel tubes used in the heat exchanger (gas cooler) under significantly higher pressure and temperature. In addition to the static burst failure, creep and fatigue behavior have also become a concern as a result of these severe service conditions. Also any surface irregularities caused by tool workpiece interaction during extrusion can affect the fatigue behavior. Since the bulk material properties cannot be trusted as mentioned earlier, an apparatus to directly measure the static, creep and fatigue material properties under simulated service conditions is required.

1.6 Objectives

The main objective was to design and fabricate an apparatus and to generate test procedures to measure the mechanical properties of micro channel tubing used in climate control systems with CO_2 refrigerant. Based on the data obtained, the following secondary objectives are also studied.

- Variation of mechanical properties within the operating temperature range of climate control systems with CO_2 refrigerant.
- Effect of thermal brazing on mechanical properties.
- Verification of an analytical model of micro channel tubing relating the internal pressure and effective stress.
- Comparison of failure stresses from uniaxial tensile and failure stress from static burst pressure.
- Analysis of fatigue and creep behavior of the micro channel tubing.

1.7 Thesis Outline

The first chapter provided an introduction and some relevant background information that motivated this research work. The second chapter deals with the design of micro channel tube. An existing formula relating the internal pressure and the strain distribution at the tube is modified in this chapter. The accuracy of the modified formula is checked with finite element analysis. In addition some other issues related to design are discussed in this chapter.

A literature review is presented in Chapter 3. The fourth chapter describes the test apparatus and Chapter 5 explains the burst tests used in this work. This includes a static burst test, a sinusoidal cyclic test and a cyclic test with hold times.

Results and discussion are presented in Chapter seven. In the last chapter, conclusions and some recommendations for future work are presented.

As mentioned earlier, the tube samples are subjected to internal pressure and elevated temperature via the apparatus simulate the operating conditions. In other words, test samples are pressurized to failure at various temperatures and both parameters are recorded to evaluate the response.   In the next chapter, an existing formula relating the internal pressure applied to a micro channel tube to stress distribution at the section of the tube susceptible to failure is modified and simplified.

CHAPTER 2

DESIGN OF MMP

This chapter deals with issues related to design of micro channel tube and an existing equation relating internal pressure to the stress distribution at the web of a micro channel tube.

2.1 Mass and heat transfer

Much research work has been done from the standpoint of heat and mass transfer in micro channel tubing with previous refrigerants and also with CO_2 as the refrigerant. The primary aim of these efforts was to generally investigate the heat transfer in micro channel tubing and to optimize the heat transfer. This area of research has received wide attention as heat transfer in micro channel tubing is used not only in climate control systems but also in other specialized applications such as microelectronics, bioengineering and microfabricated fluidic systems. Micro channel tubing with different channel geometries such as circular, rectangular shapes with various dimensions have been suggested to optimize the heat transfer while keeping the volume of the tube at minimum [14]. As some of the tube geometries are proprietary of particular designers, rival companies also conduct research to develop their own channel geometries.

2.2 Mechanical design

As the operating conditions (pressure and temperature) had been significantly less for previous refrigerants, mechanical failure or local deformation under working conditions was not a serious concern for the designers. As previously stated, the switching to CO_2 makes the operating conditions stern. Hence mechanical failure has to be anticipated and taken into consideration at the design stage. Not only must the tubing be able to withstand direct internal pressure safely but also it should not fail due to fatigue and creep under the service conditions. Information in the open literature on designing micro channel tubing based on structural criteria is limited.

A geometrical model was proposed in [15] to predict the material response and pressure at failure for micro channel tubing with rectangular channels. A formula relating the maximum pressure at the internal walls (webs) with geometrical parameters and material properties for tubing with rectangular channels was derived. The stress state at the wall (web) of the tubing is due to the internal pressure. Figure 2.1 shows the pressure acting on the rectangular channels and resulting stress state at the web.

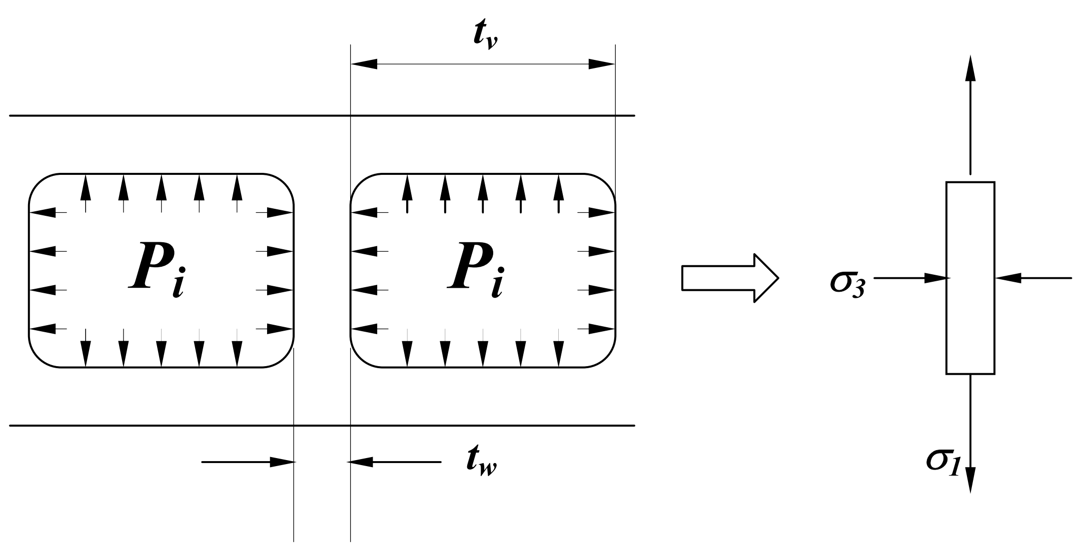

Figure 2.1: Schematic of MMP and the stress state at the wall.

These tubes generally fail when one of the webs fails. Therefore the stress state at the web was taken into consideration. Plane strain was assumed for the analysis. The material was modeled using the power law hardening equation. Uniaxaial tensile test results were used to calculate the parameters associated with power law hardening.

Based on the von Mises criterion, the maximum pressure an MMP tube with rectangular channels could withstand was given by:

$$P_{i\,\max} = \frac{2}{\sqrt{3}} K \varepsilon_i^n \left\{ \frac{s t_{wi}\left(1 - e^{-0.866\varepsilon_i}\right) + t_{vi}}{t_{wi} e^{-0.866\varepsilon_i}} + 1 \right\}^{-1} \qquad (1)$$

where K is a material constant, s is a geometry constant, n is the strain-hardening exponent, ε_i is the true strain at instability, t_{vi} is the initial width of the void and t_{wi} is the initial thickness of the web.

Experimental results from uniaxial tensile stress and static burst testing verified the validity of equation 1 [15].

2.2.1 Künesh method

Künesh derived another formula for stress at the web [16]. He considered the MMP tubing as a series of parallel individual tubes of circular or rectangular channels. By superimposing the pressures acting on two adjacent channels on both sides of the web in the middle of the two channels, he derived a formula for the effective stress at the web.

Since the samples used for the current research work is tubes with circular cross section, the tube with circular channel is considered here. Künesh method is to be applied with sight modification and the resulting relationship is simplified in the following section.

The tangential stress (σ_t) distribution along the wall of an internally pressurized cylinder is shown in Figure 2.2.

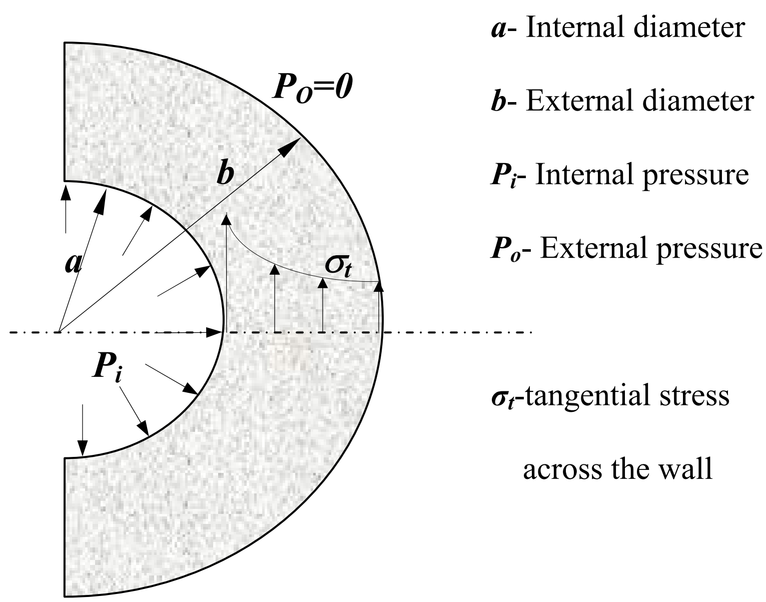

Figure 2.2: Tangential stress distribution.

The tangential stress at a distance *r* from the center of an internally pressurized cylinder (with no pressure outside) is given by:

$$\sigma_t = \frac{a^2 p_i}{b^2 - a^2}\left(1 + \frac{b^2}{r^2}\right) \qquad (2)$$

The micro channel tubing with circular channels can be considered as a series of parallel circular tubes as shown Figure 2.3.

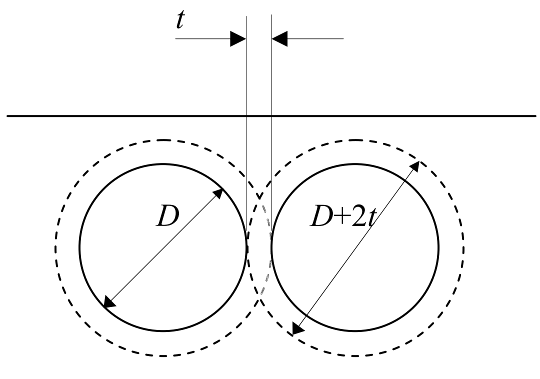

Figure 2.3: Superpositioning of two cylinders in an MMP tubing.

Starting with Equation 2 for the tangential stress at a point distance ***r*** from the center of the cylinder, the resulting tangential stress at that point due to superposition of the two adjacent channels could be expressed as:

$$\sigma_t = \frac{a^2 p_i}{b^2 - a^2}\left(2 + \frac{b^2}{r^2} + \frac{b^2}{(a+b-r)^2}\right) \qquad (3)$$

where $a = D/2$ and $b = (D+2t)/2$.

The average tangential stress across the web could be found by integrating the tangential stress and dividing it by the corresponding area (as given in Equation 4).

$$\sigma_1 = \sigma_{t_{ave}} = \frac{2}{b-a}\int_a^b \sigma_t dr \qquad (4)$$

Assuming plain strain conditions, the resulting equation for stress is

$$\sigma_{t_{ave}} = \frac{2aP_i}{b-a} = \frac{DP_i}{t} = \sigma_1 \qquad (5)$$

Neglecting the variation of radial stress in the radial direction,

$$\sigma_3 = -P_i \qquad (6)$$

The effective stress is given as.

$$\bar{\sigma} = \frac{1}{2}\left[3\left(\sigma_1^2 + \sigma_3^2 - 2\sigma_1\sigma_3\right)\right]^{\frac{1}{2}} \qquad (7)$$

After substitution and simplification,

$$\bar{\sigma} = \frac{\sqrt{3}}{2}P_i\left(\frac{D}{t}+1\right) \qquad (8)$$

where P_i is the internal pressure, D is the diameter of circular channel and t is the thickness of the web.

When designing a product based on failure criteria, the material properties such as Young's modulus, yield strength and Poisson's ratio are required. If the material properties of the end product are not different from the material properties of the bulk material, the bulk material properties could be used for design calculations. During the manufacture of micro channel tubing, the alloy undergoes several processes before being put into operation as a micro channel heat exchanger. These processes change the material properties of the alloy. This was discussed in detail earlier in the section 1.4. Hence using the bulk material properties of the alloy for the design calculations is not appropriate.

2.3 Validation of the equation for effective stress

The effective stress at the internal wall corresponding to the failure pressure was calculated using Equation 8. In order to support the accuracy of the derived formula, the stress distribution at the web corresponding to the failure pressure was obtained using finite element analysis. As an example the equivalent von Mises stress distribution at an internal wall obtained using finite element software MSC Marc is shown in Figure 2.4 (for an internal pressure of 17.8 MPa).

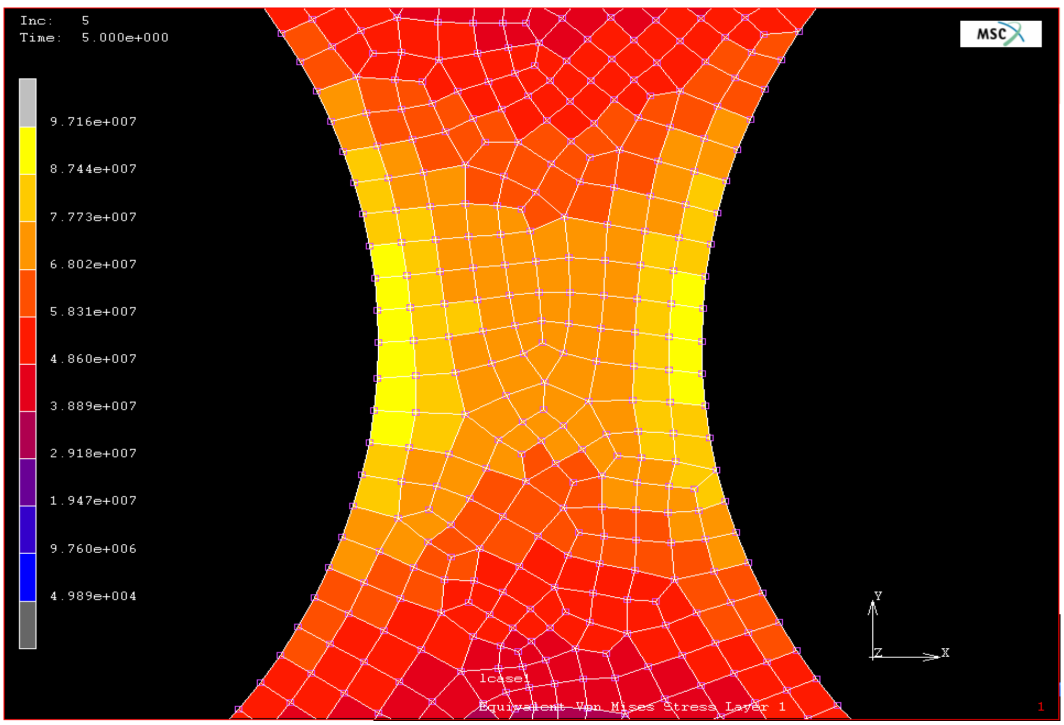

Figure 2.4: Equivalent von Mises stress distribution at a web obtained by FEA for the failure pressure of 17.8 MPa.

The equivalent stress value obtained from Equation 8 for the same pressure is 84.3 MPa, which matches with the stress distribution obtained by FEA as shown in figure 2.4. The FEA gives an equivalent stress range of 87.44-97.44 MPa (103.7% to 115.6 % of the stress value obtained from Equation 8) at the elements near the edges (shown in yellow) of the webs. The elements at the next layer (shown in yellowish orange) have an equivalent Von Mises stress range between 77.73-87.44 MPa (92.2 % to 103.7 % of the stress value obtained from Equation 2). The Von Mises equivalent stress range at elements at center (shown in orange) of the webs is between 68.2-77.73 MPa (80.9 % to 92.2 % of the stress value obtained from Equation 8). Based on the stress distribution from FEA results, the corresponding average stress was calculated to be 79.67 MPa, which is 94.5 % of the stress value obtained from Equation 8.

2.4 Other issues concerning the design

In addition to mass/heat transfer and sufficient mechanical stability against mechanical impact and pressure/temperature under operating conditions, there are some other issues such as weight, size, smoothness in operation, efficiency and cost of manufacturing need to be taken into consideration when designing the micro multiport tubing for the heat exchangers to be used in CO_2 climate control systems for automobiles.

In the next chapter, previous works on process-structure-property relationship of various aluminum alloys are discussed.

CHAPTER 3

FATIGUE AND CREEP

This chapter presents a literature review on process-structure-property relationship of different aluminum alloys.

3.1 Fatigue

As discussed in Chapter 1, the bulk material properties could not be used for design calculations of micro channel tubing. There are some additional issues that make it necessary to test the fatigue and creep properties under the simulated operating conditions. Generally, fatigue failure initiates at the surface or at a point with inclusions or defects that causes stress concentrations. As the tubing is produced by extrusion, the roughness of the internal surface is not similar all over the surface. Therefore failure initiation of the tube might be different from standard specimens used for obtaining fatigue data of the material.

A critical value of stress must be exceeded over a certain finite depth of a component for the fatigue failure to occur [17]. Particularly for the case of tubing with circular channels, the FEA had shown that the stress concentration is higher at the edge of the webs than at the interior. Due to the geometry of the tubing and the resulting stress distribution, this might make tubing behave differently from the standard specimens.

3.2 Creep-Fatigue interaction

Creep is the progressive deformation of a material at a constant stress. The operating conditions of the microchannel tubing consists of alternate pressure increase and decrease along with temperature variation. Therefore the creep-fatigue interaction of the material has to be taken into account when designing the microchannel tubing for climate control systems with CO_2 refrigerant.

More than 100 models or variations have been proposed to describe the creep-fatigue interaction. Reference [18] lists the following three as the most widely used fatigue-creep interaction models:

1) time-and cycle-fraction rule from the ASME Code Case N-47-23 [19]
2) strain-partitioning (SRP) and its total strain version [20]
3) Continuous damage mechanics [21].

3.3 Methods of testing

Applying repeated cycles of loading with hold periods at maximum load alone or minimum load alone or in combination is the most common method of creep-fatigue testing. Applying alternate periods of creep and fatigue loading is another method of testing but that is seldom used.

3.4 Previous studies

The fatigue and creep properties of aluminum alloys, specifically used in aerospace applications, have been studied widely.

Srivatsan [22] tested the tensile and the fatigue properties of AA 7055. The samples he had used came from ALCOA after a proprietary thermo mechanical treatment consisting of solution heat treatment, water quenching and permanent stretch prior to artificial aging at 190 C. The tensile strengths were measured at 27C, 100C and 190 C in longitudinal (rolling direction) and transverse directions. His results showed that the yield strength in transverse direction is slightly greater than that of longitudinal direction at 27 C and 100C. But they were equal at 190 C. Axial stress amplitude tests with a stress ratio (R) of 0.1 and axial strain amplitude tests with a stress ratio of -1 were conducted at 27 C and 190 C. His results showed that the fatigue properties vary significantly with direction and temperature. An increase in temperature had a detrimental effect on fatigue properties in the transverse direction. However the increase in temperature had a little effect on fatigue properties in longitudinal direction.

In another study, Srivatsan et *al.* [23] investigated the influence of temperature in high cycle fatigue properties and fracture characteristics of Aluminum alloy 2524. Tensile and fatigue properties were measured by mechanical testing in both longitudinal and transverse directions. These experiments were conducted at temperatures of 54C, 27C and 97C. A closed loop servo hydraulic mechanical test machine (INSTRON) with 100kN load cell was used to perform the testing of mechanical properties of the alloy. An environmental chamber was used to conduct the testing at cryogenic temperature and elevated temperature. Fatigue tests were conducted with a frequency of 5 Hz and a stress ratio of 0.1. The results showed that the yield strength and ultimate tensile strength were nearly same in longitudinal and transverse directions in T 351 condition. The cyclic fatigue life behavior of the samples in transverse direction was inferior to that of samples in transverse direction particularly at high cyclic stress amplitudes.

Shih T.S, Chung Q.Y *et al.* [24] studied the tensile and the fatigue properties of as extruded AA 7005 aluminum alloy with a rotating beam test. The samples were machined from an extruded aluminum bar of 24 mm diameter. Prior to the extrusion, a round billet of 160 mm diameter was heated to 753K and soaked for a period of time. The heated billet was extruded using a direct extrusion press rated at a maximum force of 1200 U.S tons. The relationship between stress amplitudes and cycles to failure was obtained from the experiments. Also the effect of particles or inclusions on the fatigue life of as extruded AA 7005 alloy was analyzed in this study. Their study showed that increasing particle count decreases the fatigue life of rotating bending tested samples.

Yaguchi H *et al.* [25] investigated fatigue damage in AA 3003 heat transfer tubes. Their aim was to find a parameter that could indicate fatigue damage prior to crack initiation. The samples were subjected to various numbers of fully reversed loading cycles by a hydraulically operated servo-controlled vertical tension-compression fatigue testing machine. The dislocation structures were obtained by transmission electron microscope. Development of random cells from dislocation structure was observed as the number of low fatigue cycles increased. Then the random cells changed into clear cells and finally to sub-grains. The formation of cell structures and changes in cell-wall thicknesses were related to the number of cycles the samples had undergone. A fatigue damage index was defined as the ratio between the number of cycles of loading the material had undergone in service to the number of cycles up to fracture. This parameter was found to be inversely proportional to the average cell-wall thickness.

McMaster F.J *et al.* [26] studied the influence of orientation, sheet thickness and specimen geometry on fatigue crack growth in Al-Li alloy (AA 2090). The sample material had been solution heat treated, permanently stretched to 4-6% and artificially aged to near-peak strength. A series of constant load amplitude fatigue crack growth tests were conducted using a servo hydraulic test frame with 250kN capacity. The experiments established different fatigue crack growth rates at different orientations.

Larry Byrd *et al*. [27] investigated random amplitude fatigue life of electroformed nickel micro-channel heat exchanger coupons using a shaker test. The aim of the study was to find whether the standard fatigue data for nickel could be used to predict the fatigue behavior of the coupons. Shaker tests were conducted to obtain the fatigue properties of the micro-channel coupons. Their results imply that the standard fatigue data could not be used to predict the fatigue life of micro channel heat exchanger tubing as the micro channel heat exchanger coupons have locations with stress concentrations.

However, there apparently is nothing published in the open literature on the process-structure-property relationship of micro channel tube for CO_2 climate control tube or any other extruded micro channel tube. In the next chapter, the apparatus to measure the mechanical properties of micro channel tubes will be described.

CHAPTER 4

TEST APPARATUS

The newly designed test apparatus is described in this chapter.

4.1 Experimental set-up

Figure 4.1 shows a schematic diagram of the experimental set-up.

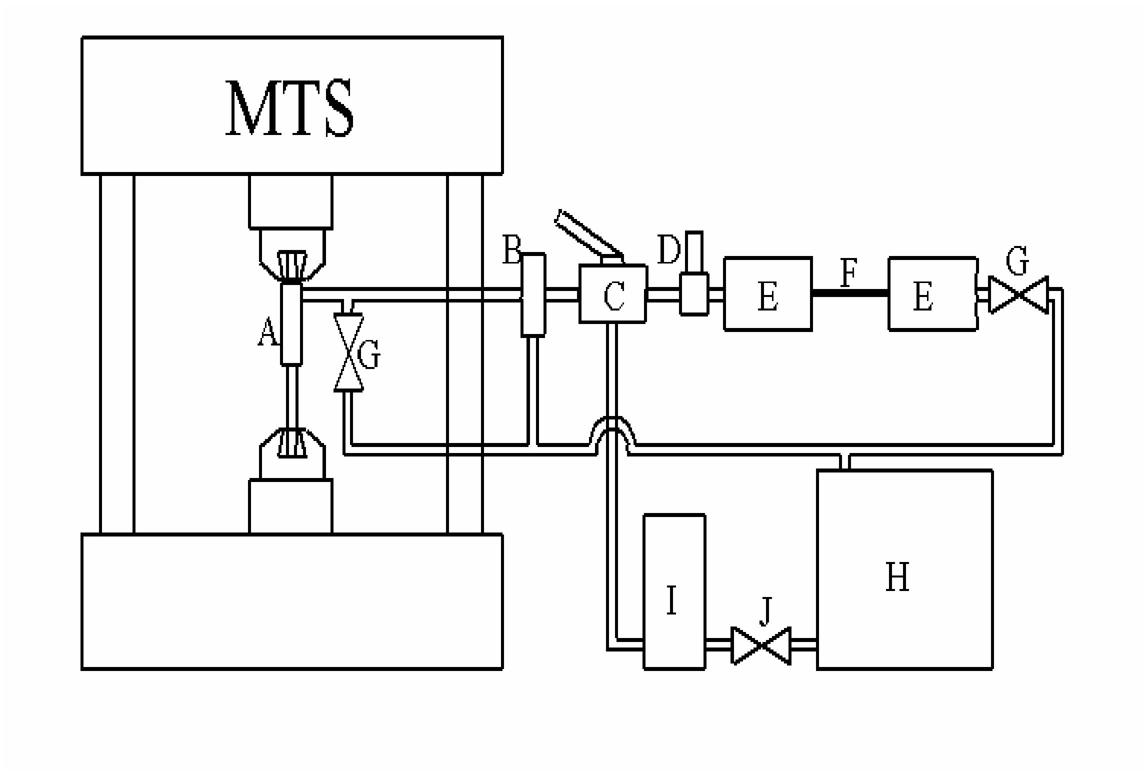

A) Single acting high-pressure cylinder. B) High pressure relieve valve. C) Three-way control valve. D) Pressure transducer. E) Quick-disconnect test fixtures. F) Micro-channel tube sample. G) Bleeder valves. H) Fluid reservoir. I) Air-operated fluid charge tank. J) Solenoid valve.

Figure 4.1: Schematic of the test set-up.

The basic idea is to generate fluid pressure and to apply that to the inside of micro channel samples. A single acting high-pressure cylinder fixed between the ram and crosshead of a servo hydraulic MTS machine generates the fluid pressure. When the MTS machine exerts force on the cylinder, the fluid inside the cylinder is pressurized. The fluid used is water mixed with undyed metalworking concentrate to prevent corrosion of the components of the apparatus. The pressure is transferred to the sample tubing held within a pair of quick-disconnect test fixtures. A pressure transducer is used to record the internal pressure dynamically. A water reservoir, air actuated water charge system and a three-way valve are in the setup to force the water into the cylinder and into the sample. Two bleeder valves are used to evacuate the air trapped inside before applying any force on the cylinder. The whole apparatus was designed to withstand a maximum pressure of 68.95 MPa (10,000 psi).

4.2 MTS Machine

The MTS machine is a model 810 type. The loading capacity is 250 kN (55kip). The hydraulic power supply of the MTS is of model 520.10B. It has a working pressure capacity of 20,684 Pa (3000 psi). The flow capacity of the hydraulic power supply unit is 38.3 l/min (10.1 gpm).

The servo hydraulic MTS machine is digitally controlled by software (Multipurpose Testware) in a personal computer. It can be programmed to pressurize the sample tubing as required. It is possible to operate the machine in different modes of control such as force, displacement etc. Also, it is possible to have different types of loadings or displacements of the ram. The software application that controls the MTS machine can be programmed to make decisions based input signals.

Figure 4.2 shows the MTS machine, the cart on which test apparatus is mounted and the PC controlling the MTS machine. The test apparatus is fixed on a cart for portability.

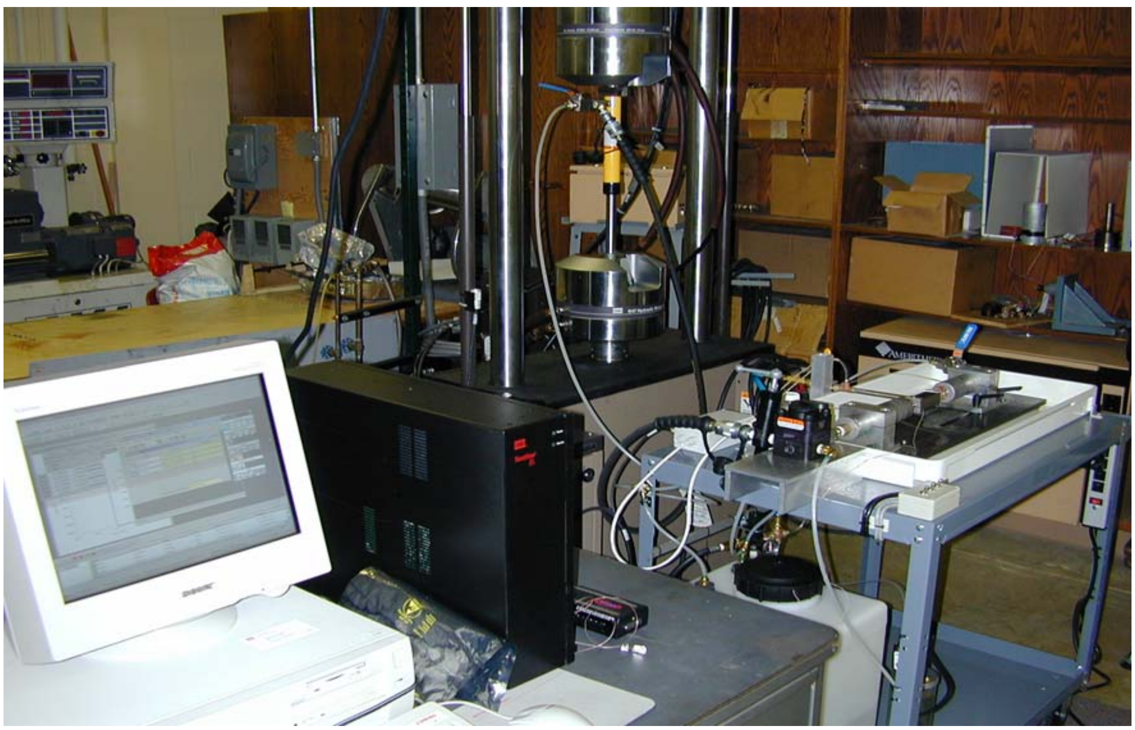

Figure 4.2: Test apparatus with the MTS machine and PC that controls the MTS machine.

4.3 Heating arrangement

A forced-air convective resistance heater was designed and incorporated into the apparatus to perform the testing at elevated temperatures simulating service conditions. A control system along with a thermocouple attached to the surface of the sample adjusts the heat generated to achieve a specified temperature.

The heating arrangement is shown in Figure 4.3.

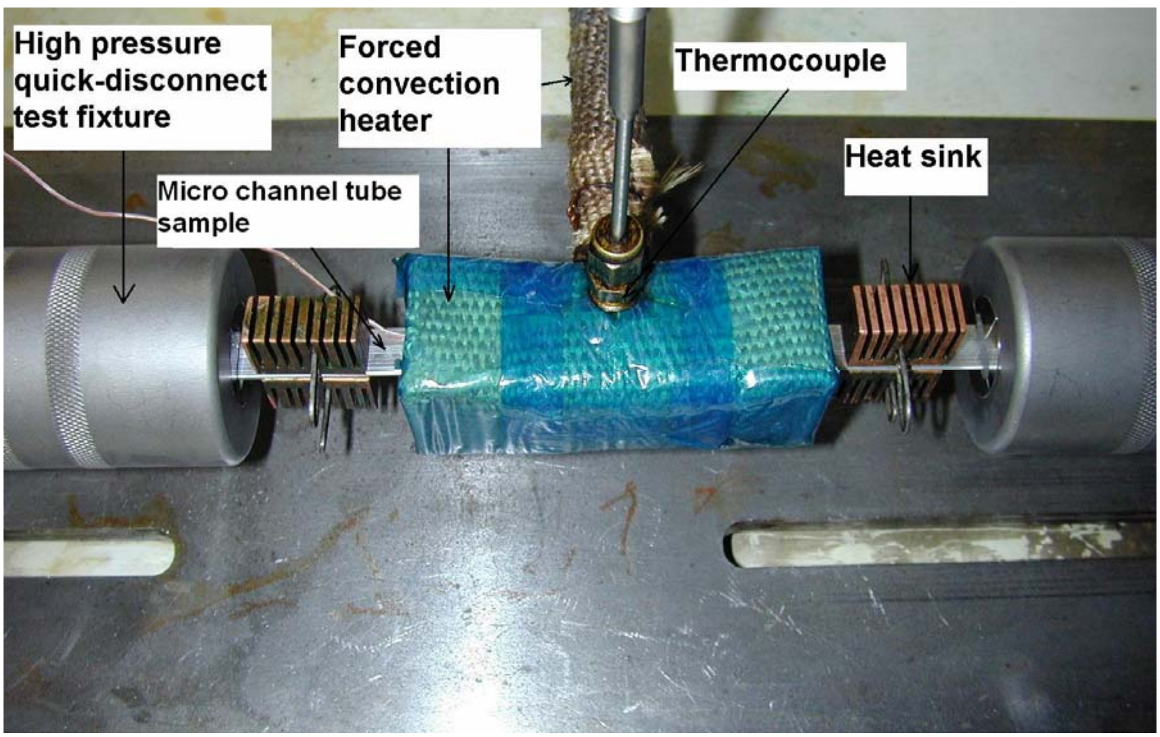

Figure 4.3: Micro-channel sample at the test set up.

Two pairs of special clip-on heat sinks are used to minimize the heat conducted to the test fixtures. The temperature of the sample can be read from the PC from another thermocouple mounted on the surface of the sample.

4.4 Sample

Burst (static) pressure tests were conducted on as-extruded tubing samples and also on samples that had undergone simulated brazing thermal cycles. The samples used in testing were made of alloy AA3102 and are of 22.5 mm in length.

Table 4.1 gives the compositions of two batches of the AA3102 samples used in this research. Brazeway Inc., performed the chemical analyses.

Table 4.1: Alloy chemistry of two AA3102 batches in weight percentage. Compositions as determined with optical emission spectroscopy (OES).

	Elements						
	Al	Fe	Mn	Si	Ti	Cu	Mg
Batch 1	99.2	0.4040	0.2383	0.0754	0.0156	0.0065	0.0134
Batch 2	99.2	0.3997	0.2250	0.0667	0.0145	0.0127	0.0169

Figure 4.4 shows a sketch of the cross section of the micro channel tubing used in the tests.

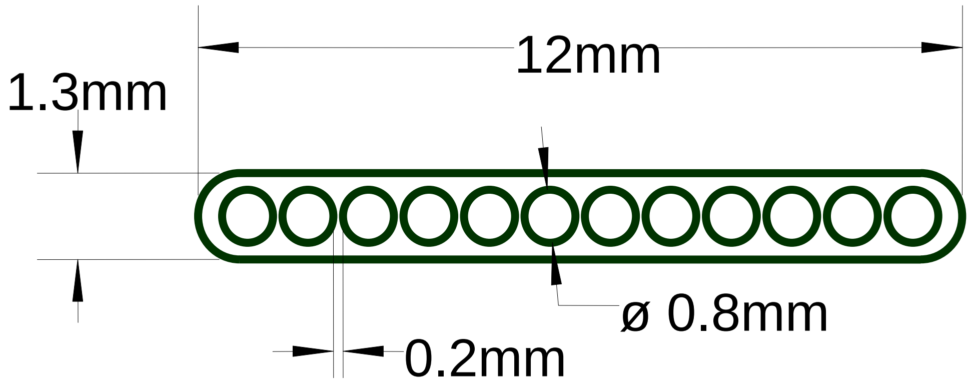

Figure 4.4: The cross section of the sample tubing tested.

As previously mentioned these tubes are thermally brazed before put into operation. In order to study the process-structure-property relationships of MMP tubing, the brazing thermal cycle was simulated in a tube furnace. The samples were held at 600˚C-605˚C for 2 minutes. The aim of this simulated thermal brazing cycle is to obtain microstructure similar to what is present in micro channel tubing in a brazed automotive condenser. Also the static pressure tests were conducted at elevated temperatures. The internal pressure, the temperature and other data such as force exerted by the MTS machine were digitally recorded.

4.5 Burst test failure of a sample

For the samples tested, failure initiates at the center of the internal walls (webs). After the failure of the internal webs, the external wall fails at a lower pressure than that at which the internal webs fail. Figure 4.5 shows a pressure-ram displacement plot obtained from a static burst test.

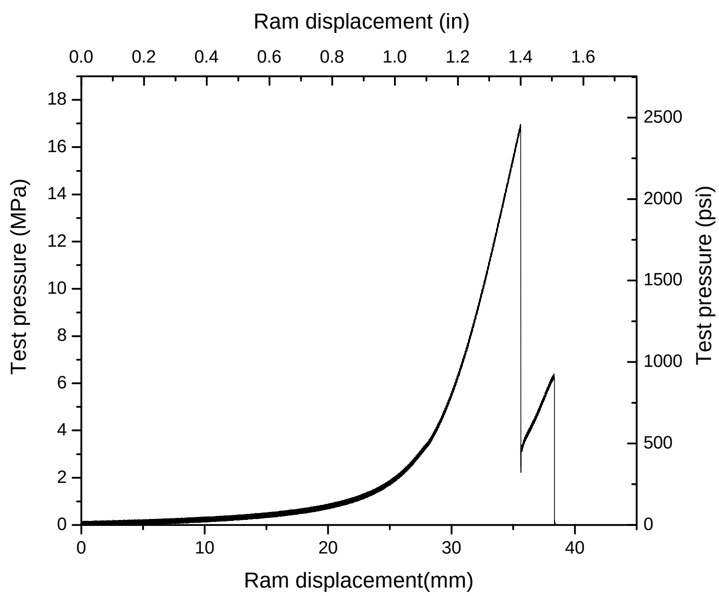

Figure 4.5: A typical test pressure- ram displacement curve obtained at room temperature for an as extruded sample tubing.

The first pressure drop corresponds to the failure of the webs and the second pressure drop corresponds to the failure at the external wall. As the failure of the web occurs first, it is enough to get the failure pressure corresponding to it. Therefore the MTS machine was programmed to terminate the test when the sudden pressure drop associated with the web failure is sensed.

In the next chapter, test procedures for the apparatus corresponding to static and cyclic loading conditions are described.

CHAPTER 5

STATIC BURST TESTING

Teststar™ is the object-oriented software used to operate the MTS machine and to define the test procedures. A Multi Purpose Testing (MPT) procedure is created by defining and sequencing different MPT processes (objects) as required. A process is a command to define an action used in a test. In this chapter, test procedures corresponding to static burst test and cyclic loading are explained.

5.1 MTS test procedure

Figure 5.1 show the MTS test procedure used for static burst testing. It consists of three processes.

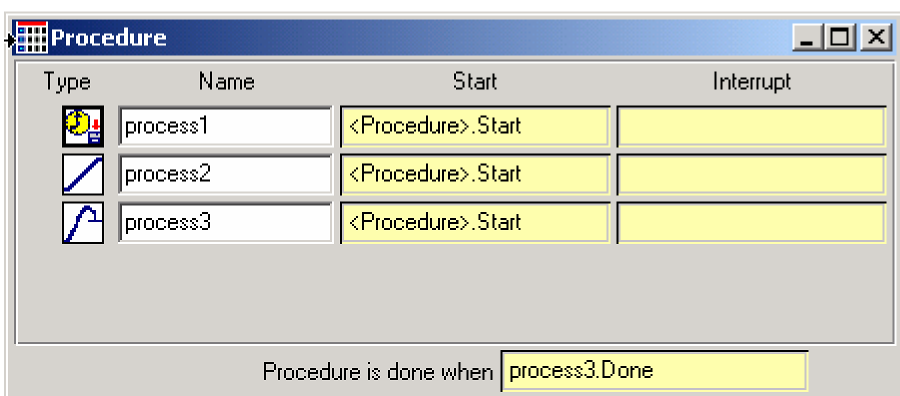

Figure 5.1 Burst test procedure.

The first process (process 1) defines the timed acquisition action. Destination folder, rate of acquisition, signals to be recorded and their units are specified in this process. Process 2 is a segment command. This defines a monotonic function to define the force to be applied by the ram or the motion of the ram. The control mode, the shape, rate or time and absolute end level are defined in this process.

For the static burst test procedure, this process is defined as a ramp function in displacement control mode. The effective cross sectional area of the cylinder is approximately 25.4 mm^3. The ram was set move at a rate of 2.54 mm/sec, and the resulting flow rate of fluid inside the cylinder was 64.5 mm^3/sec.

Process 3 in this procedure is a failure detector. This is to detect failure and to automatically stop the procedure. The criteria to detect the failure and the action to be taken upon detecting failure are specified in this process. The criterion for failure is defined as a 5% reduction in pressure from its maximum value. The application reads the pressure from an external input device.

Since all the three process have to be started simultaneously, they have been set to start accordingly.

5.2 Failure of tube

Figure 5.2 (a) shows the cross section of a micro channel tube sample before failure. Figure 5.2 (b) shows the cross section of a failed micro channel tube.

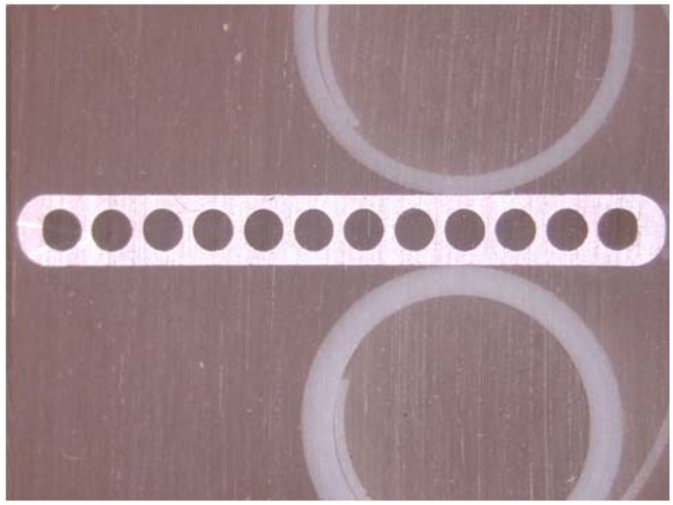

Figure 5.2(a): Cross section of the MMP tubing before failure.

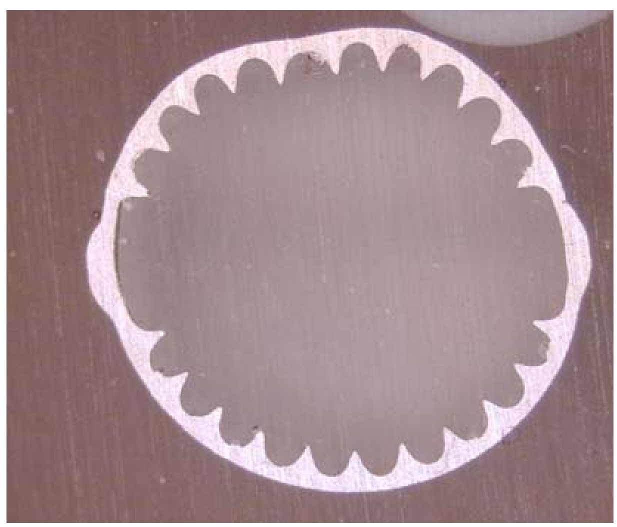

Figure 5.2(b): Cross section of the MMP tubing after failure.

Considering the geometry of micro channel tubing used for the experiment, it can be determined that the stresses in the internal webs are significantly more than that in the external walls. The tubes failed at the web as expected. Since it is obvious that the failure had initiated at one of the internal walls, it is enough to consider the effective stress in the internal web for analysis and design purposes.

5.3 Analysis of a typical test pressure-ram displacement curve

A typical test pressure-ram displacement curve to failure is shown in Figure 5.3. The ram displacement was obtained directly from the MTS machine. The test pressure was obtained from the pressure transducer attached to the apparatus.

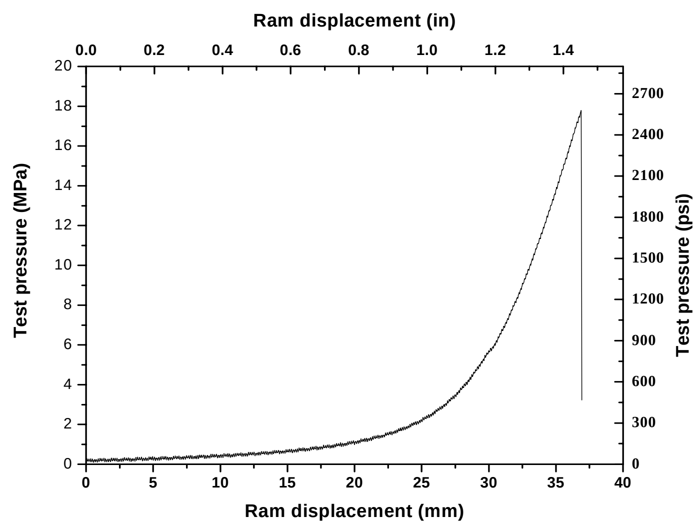

Figure 5.3: A typical test pressure - ram displacement curve obtained at room temperature for an as extruded sample tubing.

A linear portion before reaching the maximum pressure can be seen. The non-linearity up to about 32mm ram displacement is due to the compliance of the system. As the failure is very abrupt, the effective stress corresponding to failure will be calculated and compared to the results of tensile testing.

5.2.1 Fatigue testing

According to proposed material related design criteria and test methods for components driven by R 744 refrigerant, for the system to function for a lifetime of 15 years without fatigue failure, it should be able to withstand 131,000 cycles of loading with 16 MPa and 10 MPa as maximum and minimum pressures respectively [9].

In order to generate fatigue data to be used for design and that are based on the proposed criteria, fatigue experiments should have a stress ratio corresponding to a maximum pressure of 16 MPa and a minimum pressure of 10 MPa. Therefore all the fatigue loading cycles should be of the same stress ratio of 0.625.

5.2.2 Test procedure for fatigue testing

Once a specimen directory is created in the software application called “station manager”, a corresponding test procedure has to be created incorporating required functions. As mentioned earlier, an MPT test procedure is created by defining and sequencing different MPT processes (objects) as required.

Figure 5.4 shows the processes defined to run the cyclic loading test for measuring the fatigue properties of micro channel tubing. This procedure consists of 4 objects and corresponding parameters.

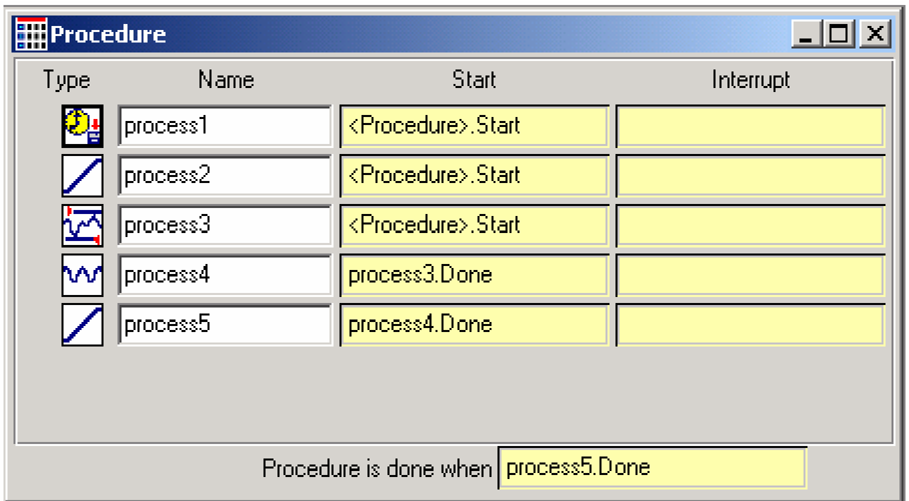

Figure 5.4: Fatigue test procedure.

As stated earlier, “process 1” invokes and defines and defines data aquisitation. The internal pressure is measured by the pressure transducer. The internal pressure and the time are the most important parameters to record. The data is recorded at a rate of 100 readings per second. Once all the parameters are established for the required loading cycle, the MTS machine is capable of generating identical loading cycles as long as there is no failure or leakage in the apparatus. The data is recorded for the entire duration of every test. As with the static burst tests, different file names have to be specified for each test.

"Process 2" (of Figure 5.4) is a segment command to define a monotonic function to specify the force to be applied by the ram to the cylinder. The control mode, the shape of the function, the rate or time and the absolute end levels were defined in this process. This is specified so that the pressure inside can reach a pressure level within range of the pressure cycle to be applied.

If the sample fails after a few cycles, the data file generated by process 1 can be analyzed to identify the exact point at which the failure had occurred and also to check for any changes in maximum and minimum pressure value. If the sample failed after several thousand cycles, the data recorded by the "process 1" would be a large data file. This is difficult to analyses. "Process 3" is used to record the peak and valley values of internal pressure. If a sample fails after tens of thousands of loading cycles, then the "peak-valley pressure value" file is analyzed to check whether the cycles are within the specified limits since the main concern is make sure that there are no shifts in pressure cycles. "Process 4" is to define the cyclic command. Figure 5.5 shows the cyclic command parameters corresponding to process 4.

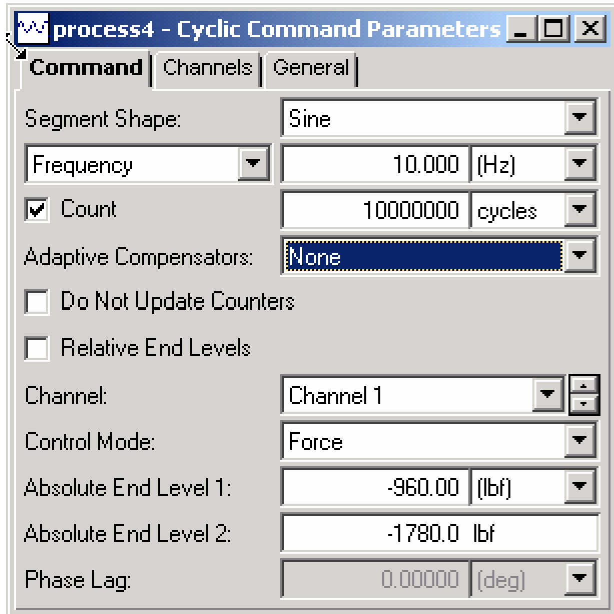

Figure 5.5: Cyclic command parameters

Since the loading cycle is sinusoidal for the fatigue testing, sine segment type is selected for this process. The frequency is specified as 10 Hz. The count is activated so that the number of applied cycles can be read dynamically during the test. As the test could run for thousands of cycles before failure, the number of cycles to run is specified as 10^6.

The control mode was selected as the force one. The test loading cycles are defined with the absolute end levels of force. By convention with the MTS machine, compressive force is negative. Since compressive force is used to generate pressure in the cylinder, negative values are used as absolute end levels of force. Trial and error values have to be assigned to the absolute end levels to obtain the required maximum and minimum pressure. A graphical software scope window is used to visualize the pressure cycle.

Figure 5.6 shows the scope window when performing trial testing with dummy samples to obtain the required pressure loading cycles. The channels were set to read and plot force reading from the load cell of the MTS machine and the pressure transducer reading. The scales, units, plot mode and trace mode were set correspondingly.

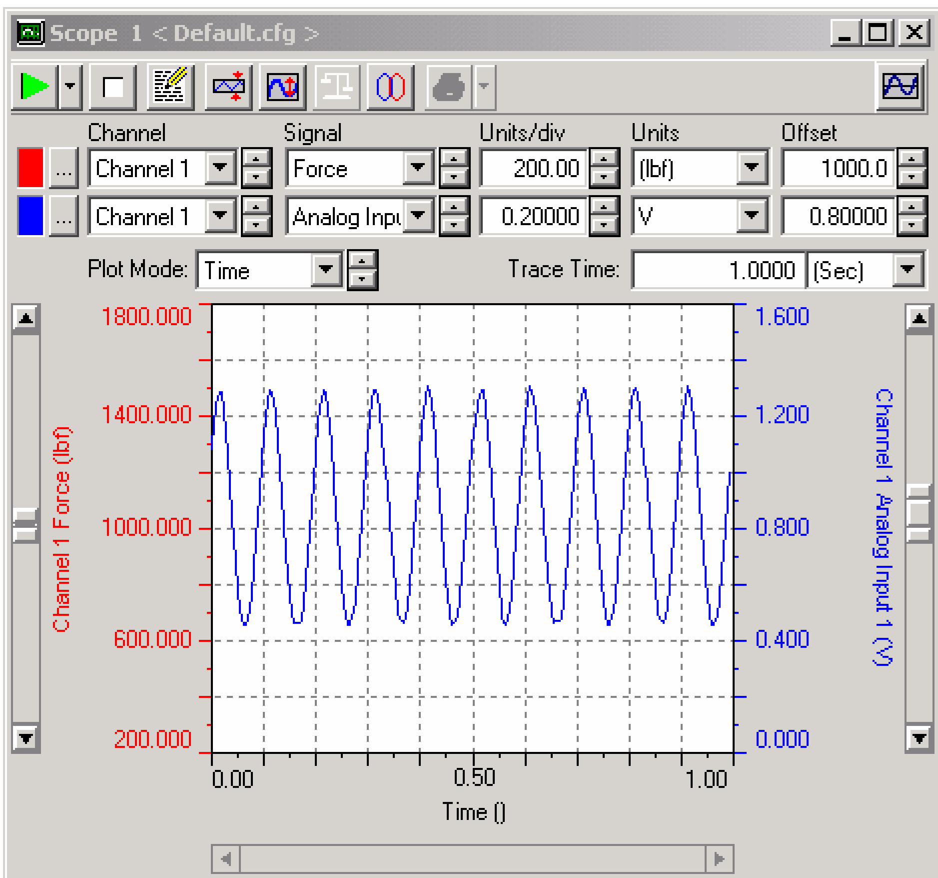

Figure 5.6: Scope window.

The scope window was set to show variation of the voltage signal corresponding to internal pressure. This value (channel 1 analog input in Figure 5.6) has to be multiplied by a factor of 1000 to get the internal pressure in psi and then by 1/145 for converting to MPa.

Also the proportional, integral, differential and feedback (PIDF) control values were adjusted to obtain the required loading cycles. Figure 5.7 shows the controls to tune the PIDF controllers. Tuning was done prior to running tests with actual samples.

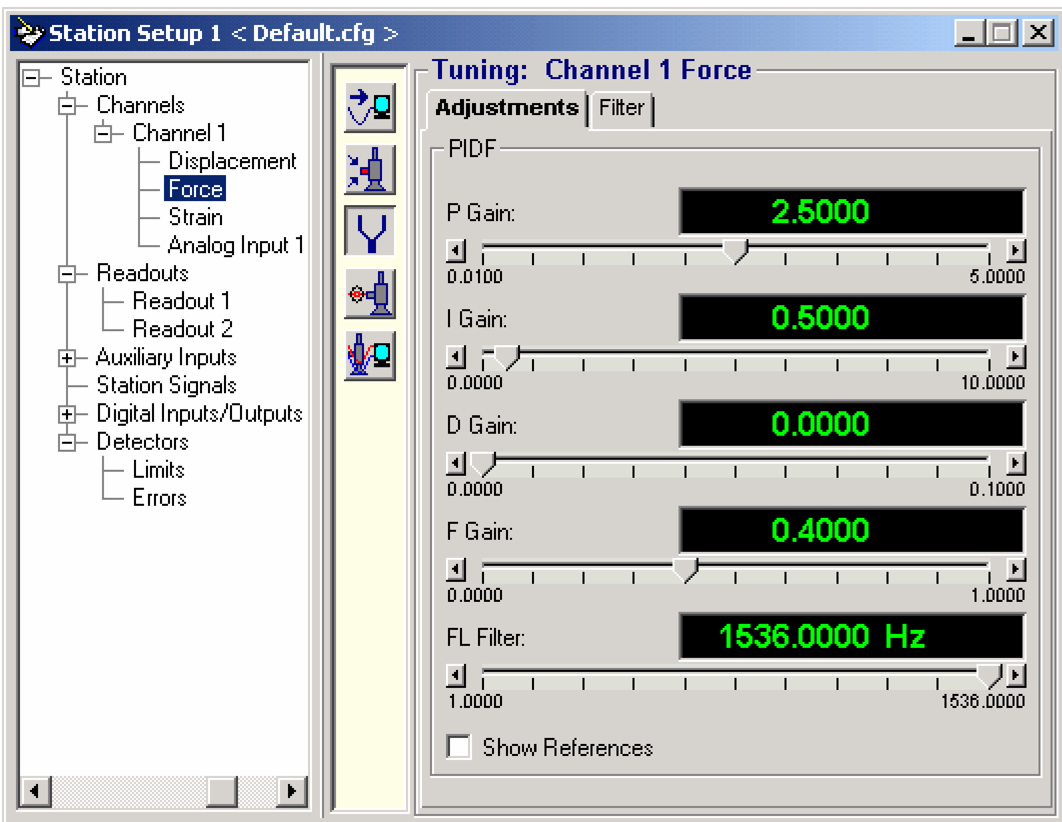

Figure 5.7: Tuning of PIDF controllers.

It was found that changing the P, I and D gain values did not produce stable loading cycles. However, increasing the F gain produced the desired loading cycle.

5.3 Creep

A proposed test for creep consists of 131,000 loading cycles of trapezoidal shape with 45 seconds as the hold time at maximum pressure and with maximum and minimum pressures as specified for the previous fatigue test [9]. However, since the test duration of this proposed creep test for one sample may go up to 1600 hours, the current work attempts to relate the fatigue properties with results of a creep test with a hold time of 10 seconds. Figure 5.8 shows the cyclic command parameter window used for creep test.

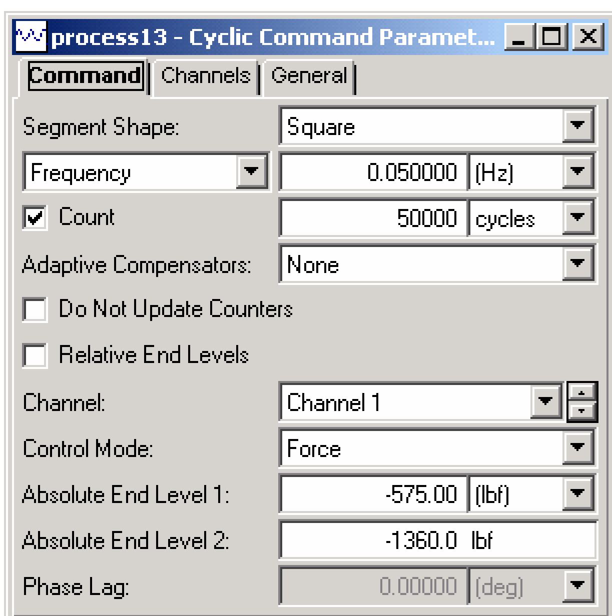

Figure 5.8: Cyclic command parameter for square segment shape.

The program for creep testing is similar to that of fatigue testing. The main difference is in "process 2". Instead of choosing the sine segment, the square segment shape was selected. As the cycle has a hold time of 10 seconds at maximum and minimum pressure values, the frequency is set to 0.05Hz. All the other processes and tuning are basically similar to that of fatigue testing.

5.4 Limit Detectors

The limit detectors display is shown in figure 5.9.

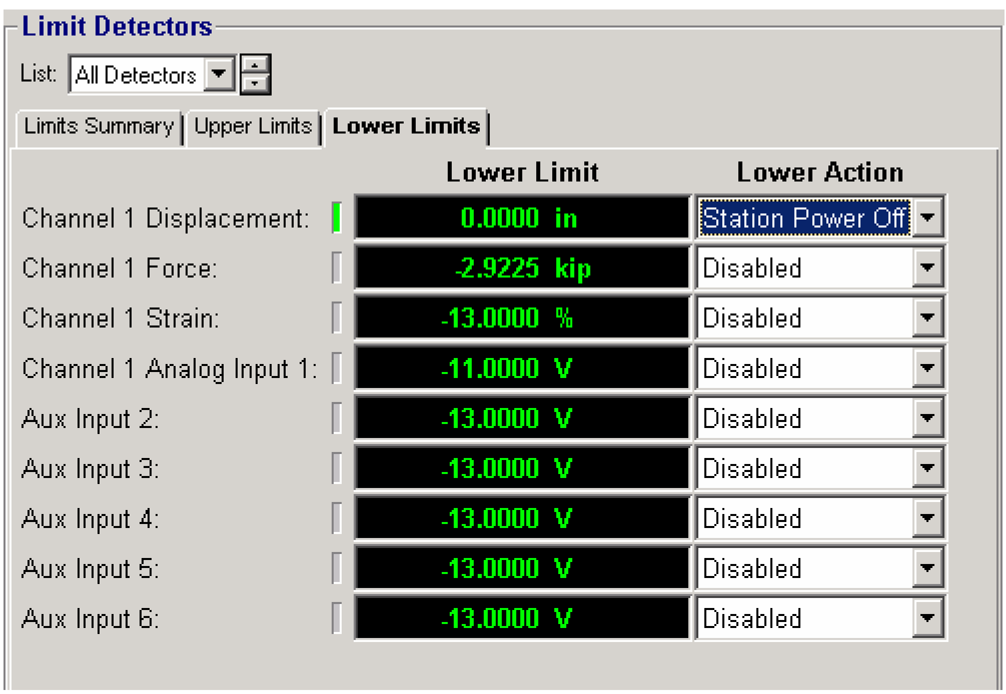

Figure 5.9: Limit detector.

Limit detectors are used to make sure that system operates within safe operating ranges of applied force, ram displacement etc. The lower limit detector for displacement was set at 0 inch as shown in Figure 5.9, so that when the ram reaches the 0 inch position due to failure or leakage, the system can turn off the power.

It can be noted that for the static burst testing, the limit detectors were not used as the criterion for identifying the failure, and corresponding action could be specified in the procedure itself. For cyclic testing, since the pressure is cyclic, the criterion for identifying failure has to be a pressure reduction below the range of pressure difference in the loading cycle. When a sample fails at a high pressure of a loading cycle, a pressure reduction equal to the amplitude of loading cycle is allowed. During this period the force exerted by the ram will not stop. This might cause some safety concern and therefore limit detectors are used.

In the next chapter, the results of these tests are presented and discussed.

CHAPTER 6

RESULTS AND DISCUSSION

The results of tests conducted for this research are presented in this chapter.

6.1 The Results of static burst testing

The results of static burst tests are discussed first.

6.1.1 The effect of thermal brazing cycle on static burst testing

Figure 6.1 compares the test pressure – ram displacement curves of an as-extruded sample and a thermally treated sample at room temperature.

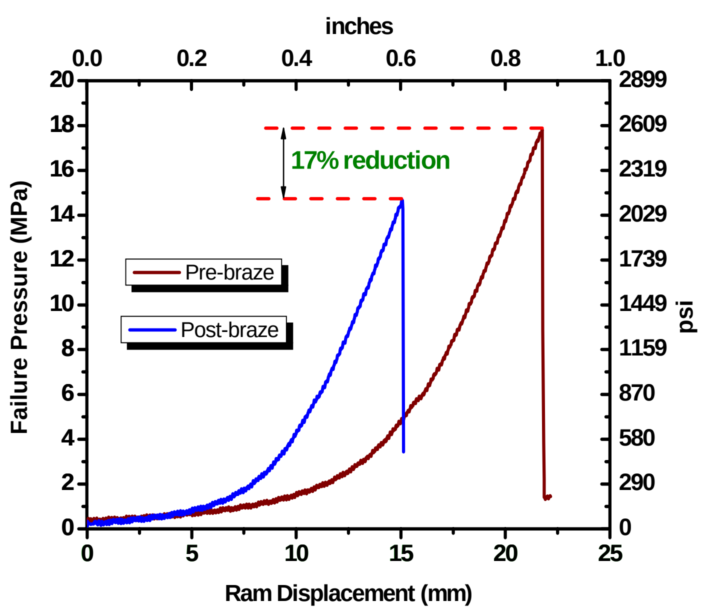

Figure 6.1: Comparison of test pressure-ram displacement of an as-extruded sample and a sample given a simulated brazing thermal cycle.

It clearly shows a reduction of 17% in static burst pressure after simulated thermal brazing.

6.1.2 Variation of failure pressure with temperature

The variation of effective failure stress with temperature is plotted in Figure 6.2.

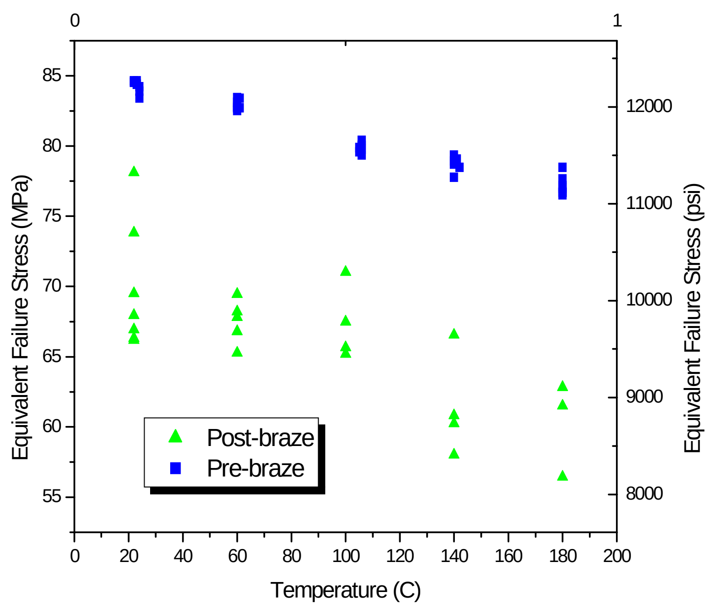

Figure 6.2: Variation of failure pressure with temperature for samples in pre and post brazed condition.

The reduction of static equivalent failure stress with the increase in temperature can be clearly seen. Reduction of static equivalent failure stress after simulated brazing is also apparent. The results of thermally brazed samples show significantly more variation than that of the samples in the pre-brazed condition.

The decrease in static equivalent failure stress with temperature of as extruded samples is 0.05 MPa/C. The samples which underwent a simulated brazing thermal cycle exhibited static equivalent failure stresses with significant variation at each test temperature.

The static equivalent failure stress of thermally treated samples decreased 0.06 MPa/C with temperature. Also, the static equivalent failure stress reduces between 17% and 22% after thermal brazing at room temperature and at 180C respectively.

6.1.3 The effect of thermal brazing cycle on uniaxial tensile testing

The stress-strain curves of samples in pre-brazed and post-brazed conditions were obtained from uniaxial tensile testing at room temperature.

Figure 6.3 shows the effect of thermal brazing cycle on uniaxial tensile testing. A significant reduction in yield strength can be observed from the plots obtained from simple tensile testing.

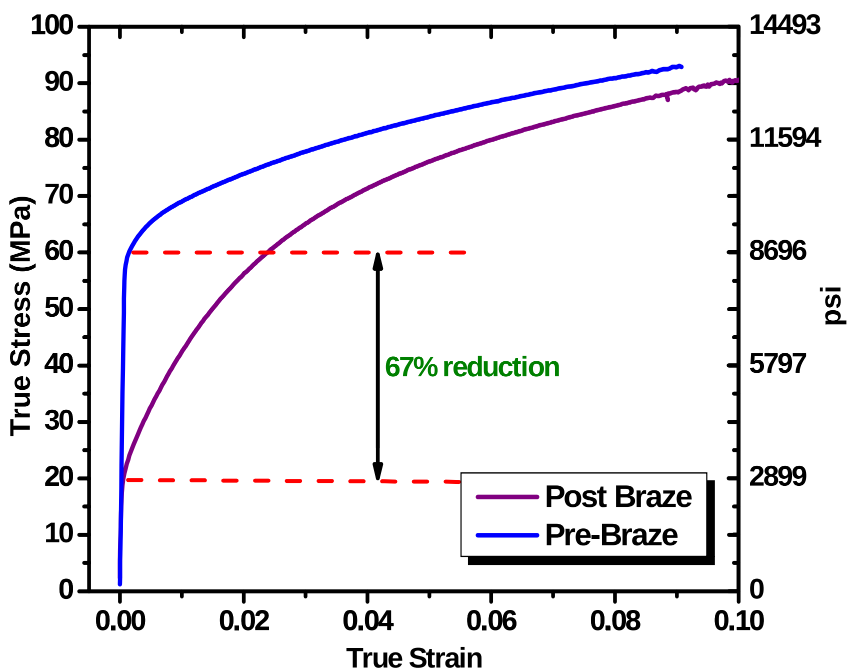

Figure 6.3: Uniaxial true stress - true strain curve of an as extruded a sample and sample that underwent a simulated thermal brazing cycle.

However there is a significant difference between the yield stresses obtained from the tensile and the effective stress obtained from the burst tests using Equation 8. Similarly there is significant difference between the effective stresses from the burst testing and ultimate tensile strength from tensile testing. Table 6.1 summarizes the results.

Table 6.1: Comparison of results from burst and tensile testing

	0.2% Yield stress (tensile test) (MPa)	Effective stress (burst testing) (MPa)	True stress at instability (MPa)
Pre-braze	57.4	84.3	102
Post-braze	27.5	69.9	110

The effective stress from burst testing was calculated using Equation 8. It seems that the burst failure occurs when the effective stress at the web is between 0.2% yield stress and true stress at instability.

6.2 Results of cyclic testing

As mentioned in chapter 5, the cyclic testing was conducted with sinusoidal loading. The first approach was to apply loading cycles at 0.9, 0.8, 0.7 and 0.6 of the static burst pressure. However a reduction of 0.1 or 0.05 of the static burst pressure seemed to be too big of a step for this case. For example, the static burst pressure of the brazed sample was 14.8 MPa (2146 psi) at room temperature. When loading cycles at 0.9 of the 2146 psi as maximum pressure were applied, failure occurred after a certain number of loading cycles.

But when loading cycles with 0.8 of the 2146 psi as the maximum pressure, were applied, the sample did not fail even after 300,000 cycles. On the other hand when loading cycles with 0.95 of the 2146 psi as maximum pressure were applied, samples failed after very small number of cycles. Therefore it was decided to vary the maximum pressure by a very small value (10-20 psi) within this range keeping the same stress ratio (R). Initially for some samples, testing was done up to 1-5 million loading cycles.

Since the frequency of the loading cycle was 10Hz, it took a significant time to complete testing. And even after those loadings, the samples did not fail. Therefore it was decided to stop the loading if the sample did not fail after 300,000 cycles of loading (duration of 8 hours).

As Equation 8 (derived in chapter 2) shows, the effective stress at the internal walls (webs) of the tubing is proportional to the internal pressure. Using this equation, the corresponding equivalent stresses can be calculated. However for simplification and comparisons, the results are presented in terms of pressure rather than the equivalent stresses at the internal walls. Also testing was conducted for only samples in the brazed condition.

6.2.1 Discussion

In the following sections some failure patterns observed from the results of the mechanical testing are discussed. Possible causes and significance of the behavior are also covered whenever necessary.

Scatter in the results, Variation from standard fatigue behavior, effect of testing temperature and effect of hold time in loading cycle are issues to be discussed.

Results of cyclic testing of the brazed samples are shown in Figure 6.4.

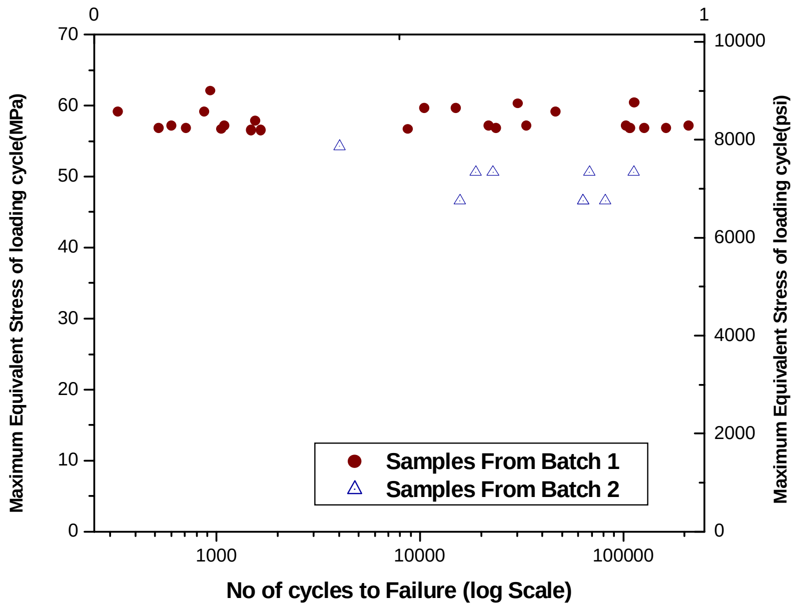

Figure 6.4: Results of cyclic testing at 90C of brazed samples from batch 1 and batch 2.

The testing was done at 90C. Samples from two batches were used for testing. The chemical compositions of these alloys are presented in Table 4.1 of Chapter 4. Since the compositions of the two alloys were different, their fatigue behavior also differs as shown in the figure 6.4.

6.2.2 Scatter in the results

Considerable scatter was seen in the results of fatigue and creep testing. In addition to scatter in the results shown, there were many samples which did not fail even after the number of loading cycles went past 300,000 and there were other samples that failed after a low number of cycles for the same loading. This scatter was within a single batch of samples. Similar to loading cycles with the same maximum and minimum stresses, the number of cycles to failure for different samples varied up to 1000 times. In other words, for loading cycles with same maximum and minimum pressures, one sample failed after N number of cycles whereas another sample failed after 10^3 * N numbers of loading cycles. Despite the fact that, high dimensional control is exercised in the production, considering the diminutive thickness of the tubing, any tiny variation or defect might have an effect upon the results. In addition, the fatigue failure initiates mostly at a surface irregularity or defects. As the samples are extruded products, any surface defects due to extrusion might have been another reason for the scatter in the results.

The process of simulated thermal brazing was done with two samples at a time. Any variation among the sample due to this might have an effect on the microstructure. This in turn might have contributed to the scatter in the results.

6.2.3 Variation from standard fatigue behavior

The Maximum stress (S)- number of cycles to failure (N) distribution from the experiments deviates from normal S-N curves of Al alloys in two aspects. Aluminum as a non-ferrous metal does not have a lower fatigue limit but in this particular case, failure did not occur for loading cycles with a maximum pressure below a certain value for the tested number of cycles. For example, at 90C, brazed samples did not fail for loading cycles with a maximum pressure value below 1710 psi. Furthermore, within the tested region, S-N curves seem to be horizontal instead of the usual curve obtained from rotating beam fatigue testing of non-ferrous metals. Experimental scatter was also rather significant, to the extent that any increase in number of cycles to failure with reduction in stress is not discernible.

6.2.4 Effects of testing temperature

Since the operating conditions of the tubes involves different temperatures ranging from room/ environment temperature to 180 C , the effect of testing temperature has to be studied.

As in the case with the results of static burst testing, the temperature at which the testing was done effects the fatigue and creep properties. Figure 6.5 compares the results of tests performed at room temperature and 90C. The specimens used in these tests had been put through simulated thermal brazing cycle. As earlier the loading cycles used for these tests also have the same stress ratio (R) of 0.625.

Even though the results are scattered, a clear decrease in the number of cycles for failure for the same type of loading cycles can be seen. At room temperature samples did not fail even after 1,000,000 cycles of loadings with the maximum pressure as 1850 psi. On the other hand, at 90C, samples did not fail after 1,000,000 cycles of loadings with the maximum pressure as 1700 psi.

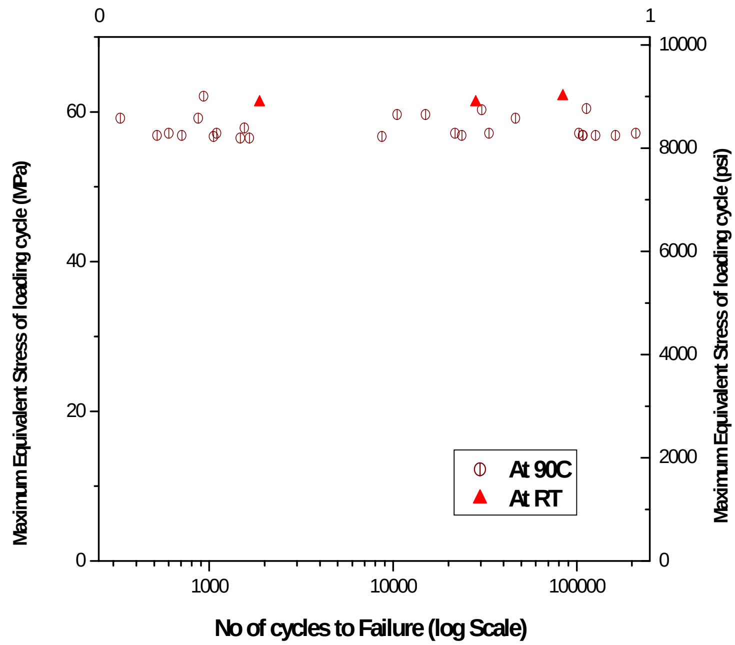

Figure 6.5: Results of cyclic testing at 90C and room temperature

Also note that at room temperature, the static burst pressure was 14.3 MPa (2074 psi). And fatigue occurs for loading cycles with maximum pressure between 2074 psi and 1800 psi.

6.2.5 Effects of hold time

Performances of the material under sinusoidal cyclic loading and cyclic loading with a hold time at maximum and minimum pressure are compared in Figure 6.6.

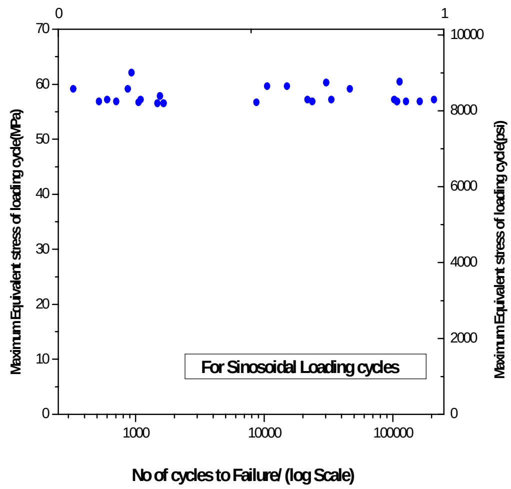

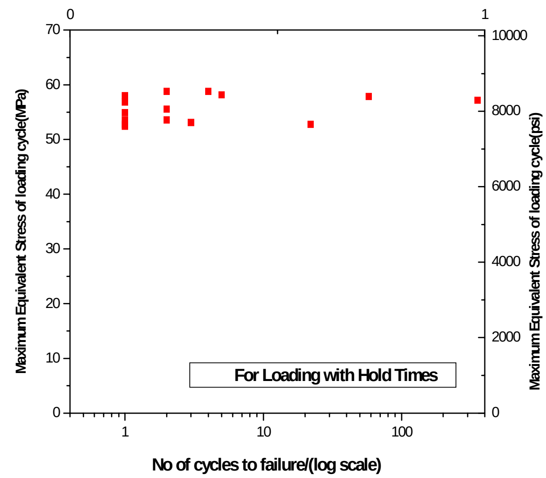

Figure 6.6: Results of cyclic testing and loading cycles with hold time at 90C

For the same value of stress ratio and maximum pressure, failure occurred with less number of cycles for loading cycles with square waveform (loading cycles with hold times at maximum and minimum pressures) than for the loading cycles with sinusoidal waveform. Also, the corresponding maximum pressures of the loading cycles are significantly less than the static burst pressure for the testing at that same temperature. This demonstrates that it is also important to consider the fatigue and creep properties of the material when designing micro-channel tubing for climate control systems using CO_2 refrigerant.

Conclusions and recommendations for future works will be presented in the next chapter.

CHAPTER 7

CONCLUSIONS

The conclusions and some recommendations for future work are presented in this chapter.

7.1 Conclusions

The manufacture of parallel flow heat exchangers for the new CO_2 based climate control systems involve processes that significantly alter material properties. This thesis specifically addresses the gas-cooler aluminum alloy micro-channel tubing through which the CO_2 refrigerant passes at high pressure and temperature after exiting the compressor, up to 16 MPa and 180 C, respectively. It is imperative to establish material property data at these operating conditions to aid engineers in design and optimization of these systems, and in particular, the geometry of the micro-channel heat exchanger tube. To this end, a special apparatus and test procedure was developed to evaluate the material behavior of micro-channel tubes for these systems. This effort was focused on the development of this apparatus in conjunction with testing of a common alloy for this application, namely AA3102. The apparatus provides precise control of internal tube pressure using an incompressible fluid (treated water), and can be used to perform static, cyclic and dynamic testing up to 69 MPa (10,000 psi). An array of such tests was performed on a current (R134a refrigerant) design micro-channel tube to characterize material behavior of the internal structural members for CO_2 system application. Testing was performed on samples in the as-extruded pre-braze condition and the post braze condition, and an analysis was performed to determine failure stresses.

- The static equivalent failure stress of as-extruded samples decreased 0.05 MPa/C with temperature and static equivalent failure stress of samples that underwent simulated brazing cycles decreased 0.06 MPa/C with temperature increase. The samples that underwent simulated thermal brazing did not exhibit consistent burst pressures at each temperature tested as opposed to as-extruded samples. In other words, brazing increases the variation in tube strength at a particular temperature. The simulated brazing process decreased the static burst pressures by 17% and 22% at room temperature and at 180 C respectively.
- A formula relating the internal pressure and corresponding maximum effective stress at the webs of the tubing was derived and the results obtained from the formula were verified with finite element analysis and they agree within 6%.
- Engineering effective stress values corresponding to static burst pressure were calculated. From uniaxial tensile testing, 0.2% yield stresses and ultimate tensile stresses were obtained and compared to burst test data for pre-brazed and post-brazed conditions. The effective stress in the web at burst was 47% and 154 % greater than the 0.2% yield stress obtained from the tensile testing at pre-braze and post-braze conditions, respectively. Similarly effective stress in the web at burst was 71% and 55% of the ultimate tensile stress obtained from the tensile testing at pre-braze and post-braze conditions, respectively.
- The results of cyclic tests show that the maximum pressure of the loading cycle decreases with temperature increase. One important pattern obtained from cyclic tests is that samples failed with fewer numbers of cycles for square waveform loading cycles than for sinusoidal loading cycle with the same maximum and

minimum pressures. The obtained S-N curves did not exhibit the conventional exponential behavior. Within the tested region, the curves are rather horizontal, indicating little influence of fatigue/cyclic loading on failure.

7.2 Future work

The results of these tests show that tubing will fail for a pressure below the static burst pressure when subjected to cyclic loading. Since the service condition of the micro channel tubing includes cyclic loading at elevated temperatures, the fatigue and creep properties of the material should be taken into consideration. As the results show the fatigue strength can be expressed as a percentage of the static strength measured from static burst testing rather than conventional S-N curve. In the future, this work can be measured for different alloys. This data will be useful not only for design of climate control systems but also in other areas such as microelectronics, bioengineering and micro fabricated fluid systems.

By doing metallurgical analysis, a better understanding of process-structure-property relationship can be attained. Tubes with different dimensions can be tested by replacing with appropriate grips. By testing tubing with different geometries, future work can focus on relating the effective stress corresponding to burst pressure to results obtained from simple tensile tests. Correspondingly relationship between fatigue behavior of the tubing due to cyclic pressure loading and conventional fatigue data of the material can also be analyzed.

REFERENCES:

[1] A fact sheet by the EPA, "Choosing and using Alternative Refrigerants for Motor Vehicle Air conditioning", May 1, 2001, http://www.epa.gov/ozone/snap/refrigerants/macssubs.html

[2] "Position of the German Automobile Industry regarding Vehicle Climate Control Use of Environment-Friendly Refrigerants", presentation, Verband der Automobilindustrie, February 7th 2003.

[3] "Innovations: CO_2 Systems", feature story, Visteon Corporation, October 4, 2001, http://www.visteon.com/about/features/2001/100401.shtml

[4] M.R. Richter, S.M. Song, J.M. Yin, M.H. Kim, C.W. Bullard, P.S. Hrnjak, " Experimental results of transcritcal CO_2 heat pump for residential application", *Energy,* volume 28, issue 10, August 2003, pages 1005-1019.

[5] "CO_2 Compressors: New Technology for Cool Heads and Warm Feet", Willi Parsch, Bernd Brunsch, 7th LuK Symposium April 11-12 2002, Germany.

[6] "New technology: CO_2 (R744) as an alternative refrigerant", Mac Summit, February 10-11 2003.

[7] "CO_2 Technologies in Japan", Nikkan Kogyo Shimbun, www.shecco.com/artikler/co2technologyinjapan.htm

[8] "CO_2 air conditioning systems", Press release, Denso Corporation, march 2002. www.desocorp-na.com/sae2002/

[9] W. Stadmüller, R. Cäsar, "Material Related Design Criteria and Test Methods for Components Driven by R744 as Refrigerant" 2000 SAE Automotive Alternative Refrigerant Symposium, July 11-13, Scotsdale, AZ.

[10] "Pressure controls for R744 climate control systems", R.Appelo, A. Kolling, H. Nijenhuis, Texas Instruments Holland BV.

[11] "Aluminum Metallurgy", whitepaper, SECO/WARWICK Corporation.

[12] "Controlled Atmosphere Brazing- The Theory", Product bulletin, SECO/WARWICK Corporation.

[13] M.M. Guzowski, F.F. Kraft, H.R. McCarbery, J.C. Noveskey, "Alloy and Process Effects on Brazed Automotive Condenser Tubing", *Proceedings of the Vehicle Thermal Management Systems (VTMS 4) Conference*, 24-27 May 1999, sponsored by the Institute of Mechanical Engineers (I Mech E) and the Society of Automotive Engineers (SAE).

[14] Y. Zhoa, M.M. Ohadi, R. Radermacher, "Microchannel Heat Exchangers with Carbondioxide", final report for the Air Conditioning and Refrigeration Technology Institute, Arlington, Virginia, September 2001.

[15] F.F. Kraft, "Method for Predicting and Optimizing the Strength of Extruded Multi-Void Aluminum Heat Exchanger Tube" *SAE 2002 Transactions Journal of Passenger Cars: Mechanical Systems*, SAE, Sept., 2003, pp.99-106.

[16] J. Künesch, "Al-extrusions for Automotive R744 Refrigerant Systems Special Material and Design Requirements", Presentation, MPA Stuttgart and Erbslöh Aluminum GmbH.

[17] George E. Dieter, "Mechanical Metallurgy", chapter 12, second edition.

[18] Gary R Halford, Bradley A. Lerch, Michael A. McGaw, "Fatigue, Creep Fatigue and Thermo mechanical life testing", ASTM handbook Code Case N-47-23, *American Society of Mechanical Engineers*, 1986.

[19] 1.S.S. Manson, G.R. Halford, M.H. Hirschberg, "Creep-Fatigue Analysis by Strain-Range Partitioning, Symposium *on Design of Elevated Temperature Environment*, American Society of Mechanical Engineers, 1971, p 12-28.

[20] J.F. Saltsman, G.R. Halford, "An update on the Total Strain Version of SRP", ASTM STP 942, *Low cycle fatigue-Directions for the future*, H.D. Solomon, G.R. Halford, L.R. Kaisand, B.N. Leis, American Society for testing and materials, 1988, p 329-341.

[21] J.L. Chaboche, "Continuous Damage Mechanics: A tool to Describe Phenomena before Crack Initiation, *Nuclear Engineering Design*, Vol 64, 1981, p 233-247.

[22] T.S. Srivatsan, "An investigation of the cyclic fatigue and fracture behavior of Aluminum alloy 7055", *Materials and design*, Apr2002, Vol. 23 Issue 2, p141.

[23] T.S. Srivatsan, D. Kolar, P. Magnusen, "The cyclic fatigue and final fracture behavior of aluminum alloy 2524" , *Materials and Design*, April, 2002 , Vol 23, issue :2.

[24] Teng-Shih Shih, Quin-Yang Chung, "Fatigue of as-extruded 7005 aluminum alloy", *Journal of materials science and engineering*, May2003, Vol. 348 Issue 1/2, p333.

[25] H.Yaguchi, H. Mitana, K. Nagano, T. Fujii, M.Kato, "Fatigue-damage evaluation in aluminum heat-transfer tubes by measuring dislocation cell-wall thickness" , *Materials science and engineering.*

[26] F.J. McMaster, C.P. Tabrett and D.J.Smith, "Fatigue crack growth rates in Al-Li Alloy, 2090. Influence of orientation, sheet thickness and specimen geometry", *Fatigue and fracture of Engineering Materials and Structures*, Feb98, Vol. 21 Issue 2, p139, 12p.

[27] Larry Byrd, Michael P. Camden, Gene E.Maddux, Alrry W. Simmons, "Random amplitude fatigue life of electroformed nickel micro-channel heat exchanger coupons", *Shock and vibrations*, 1998, Vol. 5 Issue 2, p103, 8p.

[28] F.F. Kraft, L.Huffman, G.Vamadevan, "Mechanical Testing and Analysis of Micro-Channel Tube for CO_2 Climate Control Systems", *Proceedings of the Vehicle Thermal Management Systems (VTMS 6) Conference*, May 2003, sponsored by the Institute of Mechanical Engineers (I Mech E) and the Society of Automotive Engineers (SAE).